Journal of
Synchrotron Radiation

ISSN 0909-0495

Received 12 May 2006
Accepted 4 August 2006

Performance of the atomic and molecular physics beamline at the National Synchrotron Radiation Laboratory

Sisheng Wang,[a] Ruihong Kong,[a] Xiaobin Shan,[a] Yunwu Zhang,[a] Liusi Sheng,[a]* Zhenya Wang,[b] Liqing Hao[b] and Shikang Zhou[b]

[a]National Synchrotron Radiation Laboratory, University of Science and Technology of China, Hefei 230029, People's Republic of China, and [b]Environment Spectroscopy Laboratory, Anhui Institute of Optics and Fine Mechanics, Chinese Academy of Sciences, Hefei 230031, People's Republic of China. E-mail: lssheng@ustc.edu.cn

At the National Synchrotron Radiation Laboratory, The University of Science and Technology of China, an atomic and molecular physics beamline with an energy range of 7.5–124 eV has been constructed for studying the spectroscopy and dynamics of atoms, molecules and clusters. The undulator-based beamline, with a high-resolution spherical-grating monochromator (SGM), is connected to the atomic and molecular physics end-station. This end-station includes a main experimental chamber for photoionization studies and an additional multi-stage photoionization chamber for photoabsorption spectroscopy. A mid-photon flux of 5×10^{12} photons s^{-1} and a high resolving power is provided by this SGM beamline in the energy range 7.5–124 eV. The size of the synchrotron radiation beam spot at the sample is about 0.5 mm in the vertical direction and 1.0 mm in the horizontal direction. Some experimental results of photoionization efficiency spectroscopy and photoabsorption spectroscopy of atoms and molecules are also reported.

Keywords: undulator-based beamline; atomic and molecular physics.

1. Introduction

Since the 1980s, synchrotron radiation has been used to study the photophysics and photochemistry of atoms, molecules and clusters by photoionization mass spectroscopy and photoionization efficiency spectroscopy (Kamke *et al.*, 1987; Ng, 2000; Kato *et al.*, 2006). Generally speaking, the ionization energies of most molecules and clusters are in the energy range 8–12 eV, while the photon energy is required to be as high as possible for studying the spectroscopy of atoms. In order to meet the requirements for studying the spectroscopy and dynamics of atoms, molecules and clusters, a new undulator-based spherical-grating monochromator (SGM) beamline has been constructed at the 800 MeV electron storage ring of the National Synchrotron Radiation Laboratory (NSRL) in Hefei, People's Republic of China. The beamline is designed to operate in the 7.5–124 eV photon energy range, covered with three spherical gratings and by using the first, third and fifth harmonic of the undulator inserted in the NSRL storage ring (Zhang *et al.*, 2003; Jia, 2003). This undulator, UD-1 at NSRL, has 29 permanent magnet periods and a 92 mm period length (Jia, 2003). The end-station contains the main experimental chamber and an additional multi-stage photoionization chamber. The former is used for the study of atoms and molecules, and equipped with a time-of-flight or quadrupole mass spectrometer. The latter is used for the study of absolute photoabsorption spectroscopy of atoms and molecules.

This paper is structured as follows. Following this introduction a detailed description of the undulator-based SGM beamline and the atomic and molecular physics end-station will be given in §2 and §3, respectively. In §4 the performance of the undulator-based SGM beamline will be presented and the capabilities of the end-station will be illustrated *via* experimental measurement.

2. The undulator-based SGM beamline

A schematic layout of this beamline is shown in Fig. 1 and the basic parameters of the optical elements are given in Table 1. At first, the synchrotron radiation beam from the undulator is deflected to cylindrical vertical focusing mirrors (CVFMs) by a plane horizontal deflection mirror (PHDM). The CVFM consists of both M_{VL} (for low energy) and M_{VH} (for high energy), which focus the beam onto entrance slits S_{1L} (through a plane mirror M_L) and S_{1H}, respectively. Then, the synchrotron radiation beam is diffracted by three interchangeable spherical gratings and passes through a moveable exit slit. Finally, the synchrotron radiation beam is re-focused onto the

Table 1
Optical elements of the beamline.

Optical element (see Fig. 1)	Type	Groove density (lines mm^{-1})	Radius (m)	Incidence angle (°)	Coating and blank material
M_h	Plane mirror	–	∞	86	Ni/Au Glidcop
M_{VL}	Cylindrical mirror	–	21.937	84	Au/Si
M_{VH}	Cylindrical mirror	–	32.005	86	Au/Si
M_L	Plane mirror	–	∞	77	Au/silicon carbide
SG1	Spherical grating	370	12.180	75.5	Au/Si
SG2	Spherical grating	740	12.180	75.5	Au/Si
SG3	Spherical grating	1250	15.266	78.5	Au/Si
M_P	Toroidal mirror	–	15.410 (h), 0.490 (v)	82.5	Au-coated/fused silica

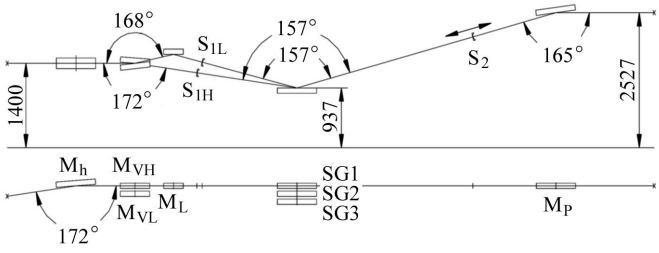

Figure 1
Optical layout of the atomic and molecular physics beamline. Dimensions are in mm where not shown.

sample by a toroidal focusing mirror. The choice of cylindrical focusing mirrors facilitates the alignment of the pre-focusing elements (PHDM and CVFM). Under the conditions of the electron storage ring in NSRL, the optical aberrations of a toroidal focusing mirror do not degrade the final image on the sample (typically 0.5 mm vertically and 1 mm horizontally).

In our beamline a grazing-incidence SGM is used and its parameters are given by Zhang *et al.* (2003). Two included angles, 151° and 157°, are employed in this SGM. The former is for the low-energy gratings SG1 (energy range ∼7.5–22.5 eV) and SG2 (energy range ∼15–45 eV), and the latter is for the high-energy grating SG3 (energy range ∼36–124 eV). The exit slit can be moved around 300 mm to keep it in focus over the energy range of the three gratings. The resolution of the three gratings has been calculated by Zhang *et al.* (2003) using the methods described by Chen (1987). The separate contributions from the primary coma aberration, entrance slit, exit slit and grating figure slope error are shown in Fig. 2. The total calculated resolution is also shown in Fig. 2. The values shown were calculated at an entrance- and exit-slit width of 80 μm for SG1 and SG2, at an entrance-slit width of 120 μm and exit-slit width of 80 μm for SG3, and figure slope error of 0.5 arcsec.

3. End-station

The end-station is composed of a main experimental chamber, an additional multi-stage photoionization chamber, vacuum system, control system, data acquisition and processing system. The main experimental chamber includes a beam source chamber, a differential chamber and an ionization chamber. The beam source chamber is evacuated by a

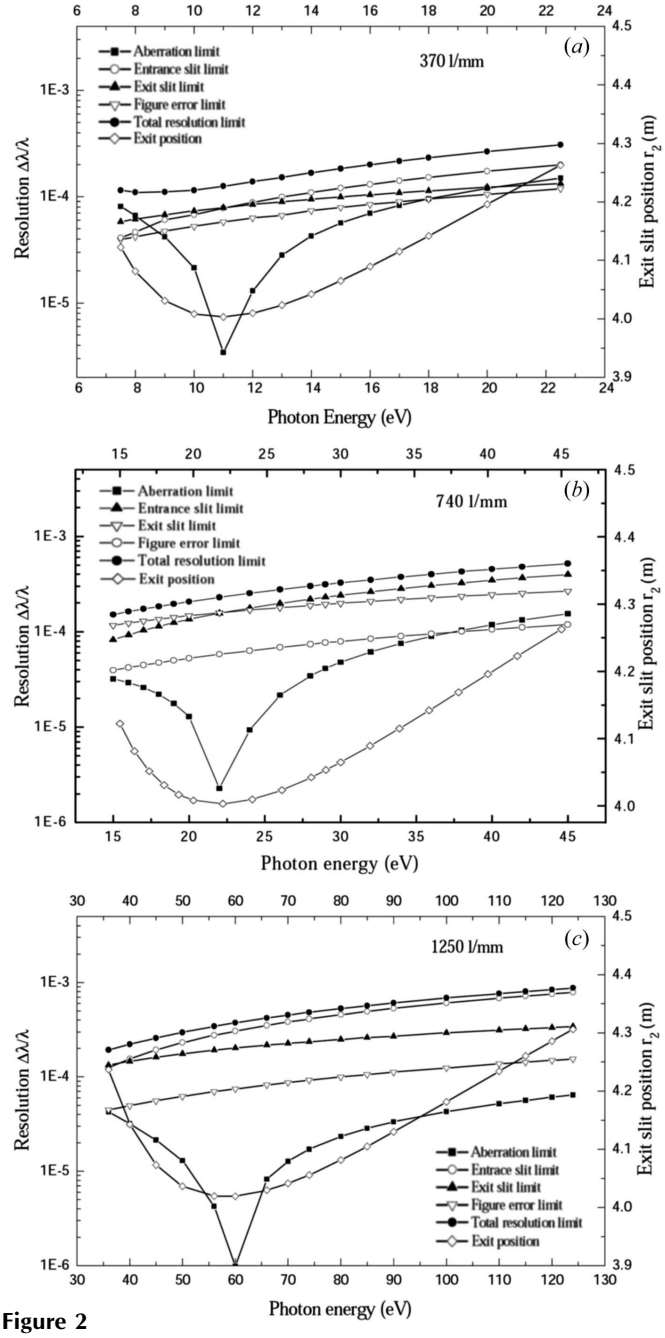

Figure 2
Various resolution limits of the monochromator and exit arm length as a function of photon energy at an entrance- and exit-slit width of 80 μm for SG1 and SG2, at entrance-slit width of 120 μm and exit-slit width of 80 μm for SG3, and figure slope error of 0.5 arcsec.

turbomolecular pump with a pumping rate of about 1500 l s^{-1}, backed by a 150 l s^{-1} scroll pump and a 15 l s^{-1} mechanical pump. The vacuum is $\sim 2 \times 10^{-5}$ Pa in the static state and $\sim 10^{-2}$ Pa during experiments. The differential chamber is pumped by a 450 l s^{-1} turbomolecular pump, backed by a 30 l s^{-1} scroll pump and a 15 l s^{-1} mechanical pump. The ionization chamber is connected to the differential chamber of the beamline *via* a differential tube of diameter 3 mm. The ionization chamber is evacuated by a 1500 l s^{-1} turbomolecular pump, backed by a 70 l s^{-1} scroll pump and a 15 l s^{-1} mechanical pump. The ionization chamber vacuum is $\sim 1 \times 10^{-5}$ Pa in the static state and $\sim 10^{-4}$ Pa during experiments.

The photoionization studies of atoms, molecules and clusters are performed using the main experimental chamber. The samples are expanded though a nozzle and two skimmers to form a supersonic molecular beam into the ionization chamber. Cooled samples in the beam are ionized by monochromatic VUV radiation at 90° in the ionization chamber and the produced ions are detected and analysed by reflection time-of-flight mass spectroscopy at 90°. The photoabsorption spectroscopy is performed using an additional multi-stage photoionization chamber (Qi *et al.*, 1997), which is connected to the main experimental chamber *via* a differential tube of diameter 3.3 mm and length 60 mm.

4. Performances of the SGM

4.1. Energy calibration of the SGM

The photon energy calibration of the monochromator was carried out using the additional multi-stage photoionization chamber and its data acquisition and processing system. In this chamber, synchrotron radiation passes through the gas between the two plates, and the electrons are attracted to one of the plates by a positive bias, while the current from the ions (repelled by the bias) is measured by the other plate using a Keithley picoammeter.

Energy calibration of the grating was carried out using the known absorption lines of some rare gas atoms and some diatomic molecules; for example, five spectral lines at 21.565 (Ne), 18.355 (N_2), 15.760 (Ar), 14.000 (Kr) and 12.120 eV (Xe) for grating SG1 (Maeda *et al.*, 1993; Hsu *et al.*, 1996; Dehmer *et al.*, 1984), five spectral lines at 45.544 (Ne), 30.850 (Ar), 28.915 (Ar), 21.565 (Ne) and 15.760 eV (Ar) for grating SG2 (Maeda *et al.*, 1993; Hsu *et al.*, 1996; Schmoranzer *et al.*, 2001; Tseng *et al.*, 1995; Schulz *et al.*, 1996), and five spectral lines at 93.810 (Kr), 91.225 (Kr), 64.816 (He), 52.474 (Ne) and 45.544 eV (Ne) for grating SG3 (Schulz *et al.*, 1996; Domke *et al.*, 1992, 1996). In the process of energy calibration the widths of the entrance and exit slits is adjusted to 80 μm and the zero-order position of the grating is determined. Then, according to those absorption peaks mentioned above, the relations between wavelength λ and position χ of the grating are determined precisely.

4.2. Energy resolution

The additional multi-stage photoionization chamber may also be used to obtain the energy resolution of the SGM experimentally. The photoabsorption spectrum near the $^2P_{1/2}$ ionization threshold is shown in Fig. 3 for 80 μm slit width, 1 meV energy steps and 20 s measurement time. Above the ionization threshold of Ar^+ $^2P_{3/2}$, one Rydberg series converges to the spin–orbit-excited Ar^+ $^2P_{1/2}$. The energy resolution of the SGM with grating SG1 can be determined directly from the line shapes of the Rydberg resonances in Fig. 3. At the 15.9 eV photon energy the resonance line width of 6.0 meV (FWHM) corresponding to a resolving power of 2700 was fitted by Gaussian peaks. The energy resolution of the SGM with grating SG2 was also evaluated with the photoabsorption spectrum near the Ar second ionization potential. The study of Ar near the $3s^23p^6 \rightarrow 3s^13p^6np$ transitions provides a good test for the monochromator resolution since the corresponding absorption transitions have extremely narrow natural line widths. We fitted these peaks with Gaussian peaks. The measured line width of the $3s^23p^6 \rightarrow 3s^13p^68p$ peak in Fig. 4 was 13.5 meV (FWHM) corresponding to a resolving power of 2100 at 28.962 eV photon energy. Fig. 5 shows the photoionization spectrum of Kr near the $3d$ thresholds measured with grating SG3. The fit of the $3d_{3/2}$–$5p$ and $3d_{5/2}$–$6p$ resonance, with the FWHM of the Lorenzian component set equal to the experimentally determined

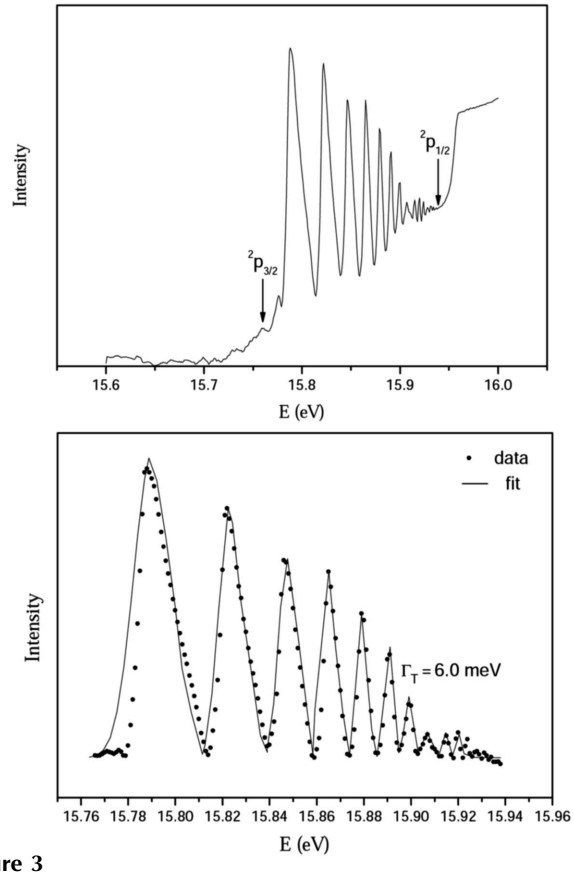

Figure 3
Photoionization spectrum of Ar near the ionization potential using grating SG1, with a 80 μm slit width and 1 meV energy steps.

Table 2
Measured resolving power compared with the calculated resolution of the monochromator, with an entrance- and exit-slit width of 80 μm.

	Resolving power	
Energy (eV)	Theoretical	Experimental
15.9	5100	2700
28.962	3200	2100
92.615	1600†	900†

† Entrance-slit width of 120 μm and exit-slit width of 80 μm.

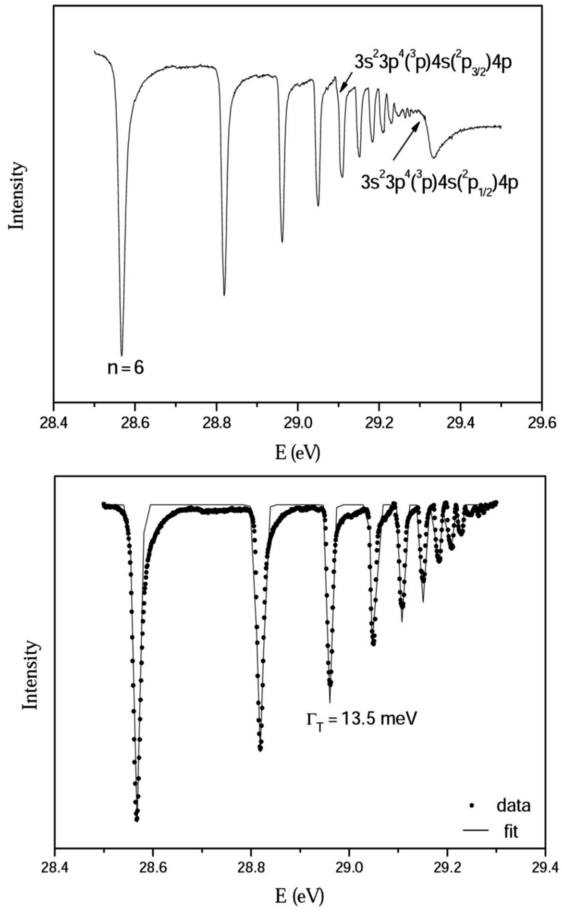

Figure 4
Photoionization spectrum of Ar $3s3p^6np$ (n = 6–∞) using grating SG2, with 80 μm slit width and 1 meV energy steps.

natural line width of 79.0 meV (Sairanen *et al.*, 1996), gives a value of the width of 102 meV about the $3d_{5/2}$–$6p$ resonance. The resolving power of grating SG3 is about 900 at 92.615 eV photon energy. Table 2 lists the measured resolving power, compared with the calculated monochromator resolution.

4.3. Photon flux

The photon flux of the beamline was measured using an SXUV-100 photodiode (IRD), which was inserted into the synchrotron radiation beam at a distance of 140 mm after the toroidal refocusing mirror. A picoamperometer (Keithley 6485) was used to measure the current i produced by the

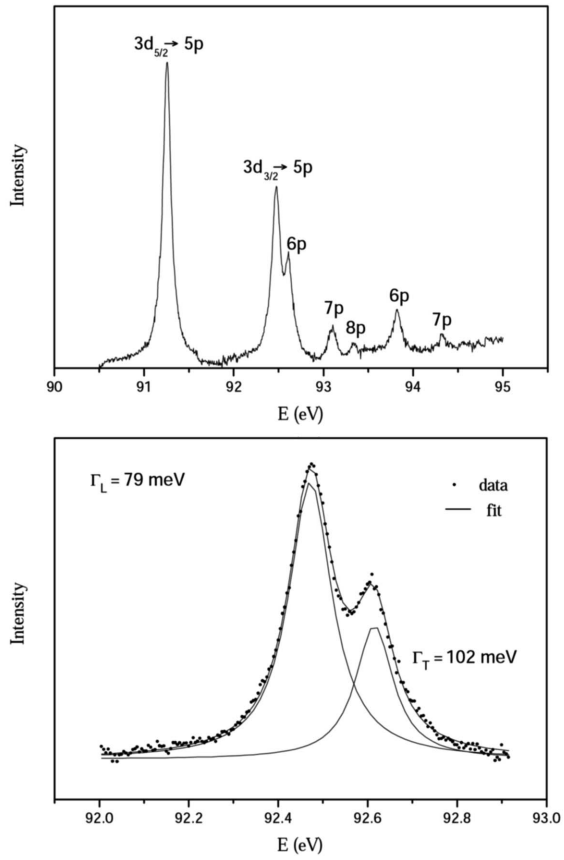

Figure 5
Photoionization spectrum of $3d_{5/2,3/2} \rightarrow np$ states of Kr using grating SG3, with an entrance-slit width of 120 μm and exit-slit width of 80 μm, and 5 meV energy steps.

photodiode. The photon flux at the sample can be calculated using

$$F\left[\text{photons s}^{-1}\,(100\,\text{mA})^{-1}\right] = \frac{1}{k\alpha(E)}\,\frac{100}{A}\,\frac{i}{e}, \qquad (1)$$

where A represents the current of the electron storage ring (in mA), e is the electron charge, k stands for the product of the transmission for the Au mesh and the fraction of whole beam detected by the photodiode, and $\alpha(E)$ is the number of electrons produced per photon as a function of photon energy. Under our experimental conditions, (1) can be reduced to

$$F\left[\text{photons s}^{-1}\,(100\,\text{mA})^{-1}\right] = 1.248 \times 10^{21}\,\frac{1}{\alpha(E)}\,\frac{i}{A}. \qquad (2)$$

The measured output flux of the beamline at an entrance- and exit-slit width of 80 μm is shown in Fig. 6. The flux peaks close to the results predicted by the theoretical estimation (Zhang *et al.*, 2003).

At the same time, a synchrotron radiation beam spot size of about 1 mm horizontally and 0.5 mm vertically was obtained *via* ray-tracing studies, and this is also the beam spot size observed for the zero order of the synchrotron radiation at the sample position.

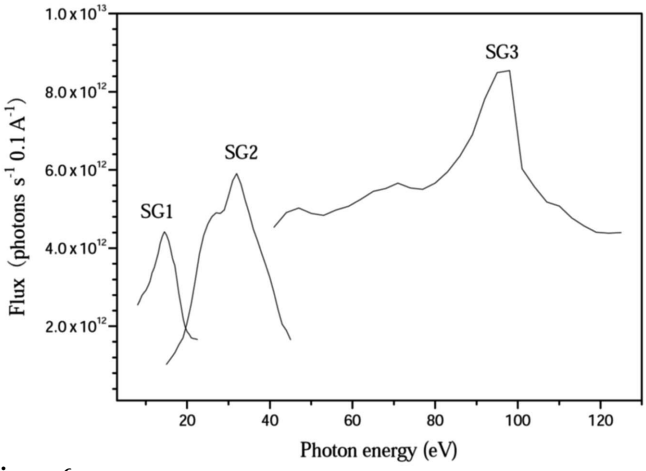

Figure 6
Photon flux measured at a fixed entrance-slit position and entrance- and exit-slit width of 80 μm.

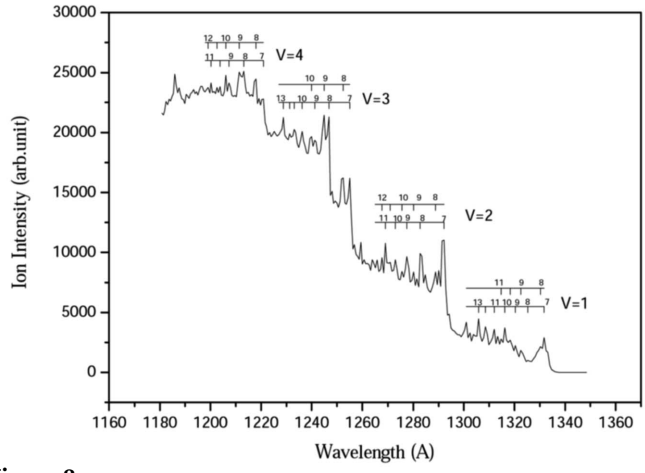

Figure 8
Photoionization efficiency spectrum of NO.

4.4. Applications of the end-station

A photoabsorption spectrum of toluene recorded using the multi-stage photoionization chamber is shown in Fig. 7. The photon energy step is 10 meV. The pressure in the absorption cell is about 0.04 torr. The measured ionization energy of toluene is 8.84 eV, which is in agreement with the data from the National Institute of Standards and Technology (NIST) of USA. The Rydberg series states, converging to B_2A' ionization threshold, are also resolved experimentally. This experimental result for the photoabsorption spectroscopy of toluene is in agreement with the result of Shaw *et al.* (1998).

In addition, the photoionization efficiency spectrum (PIES) of NO obtained using the home-made reflection time-of-flight mass spectrometer is shown in Fig. 8. Over the course of the experiment, the photon intensity was detected using a photodiode to normalize the signal of the PIES, and an MgF_2 filter was inserted into the beam to eliminate the higher harmonics of synchrotron radiation. The photon energy step is 5 meV and the ion counting time for each point is 10 s. The measured ionization energy of NO is 9.265 eV and a number of fine auto-ionizing resonant structures are also resolved in the PIES of NO. These resonant structures are assigned to auto-ionizing *np* and *ndδ* Rydberg levels which give prominent diffuse absorption bands in the spectrum. These results are comparable with those obtained by Miescher *et al.* (1978) and Ono *et al.* (1980).

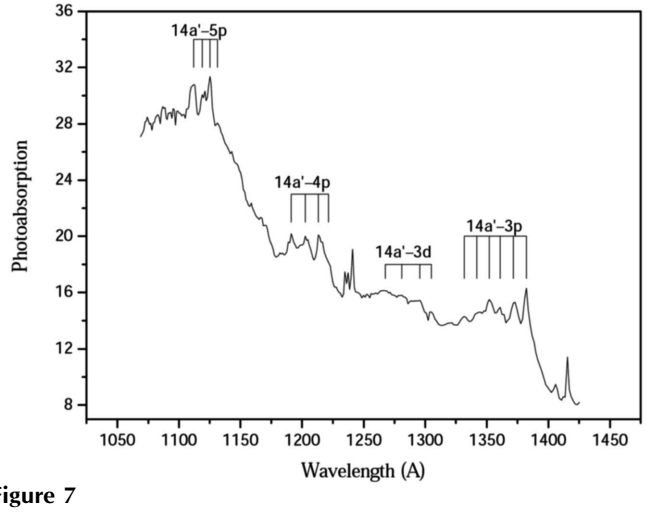

Figure 7
Photoabsorption spectrum of toluene.

5. Conclusion

A new undulator-based atomic and molecular physics beamline has been installed in the 800 MeV electron storage ring at NSRL in USTC. This SGM beamline is designed to have three interchangeable gratings with a photon energy range of 7.5–124 eV and a moveable exit slit, and operated at two fixed included angles. The performances of the SGM beamline and the end-station are evaluated by a series of spectral calibrations and tests. The energy resolution and the photon flux are good enough to meet our design requirements. The end-station is operating well now, and studies of the spectroscopy and dynamics of atoms, molecules and clusters can be performed by detecting photoelectrons, photoions and fluorescence photons. The beamline and the end-station can be used as a modern experimental research platform.

The authors would like to acknowledge Professor Fei Qi for helpful discussions. They are also grateful to Ming Yin for technical assistance and wish to thank Hui Gao for the vacuum safety system. This work is supported by the National Natural Science Foundation of China (No.10374084).

References

Chen, C. T. (1987). *Nucl. Instrum. Methods*, A**256**, 595–604.
Dehmer, P. M., Miller, P. J. & Chupka, W. A. (1984). *J. Chem. Phys.* **80**, 1030–1038.
Domke, M., Mandel, T., Puschmann, A., Xue, C., Shirley, D. A. & Kaindl, G. (1992). *Rev. Sci. Instrum.* **63**, 80–89.
Domke, M., Schulz, K., Remmers, G., Kaindi, G. & Wintgen, D. (1996). *Phys. Rev. A*, **53**, 1424–1438.

Hsu, C. W., Lu, K. T., Evans, M., Chen, Y. J., Ng, C. Y. & Heimann, P. (1996). *J. Chem. Phys.* **105**, 3950–3961.
Jia, Q. K. (2003). *High Power Laser Part. Beams*, **15**, 613–616.
Kamke, B., Kamke, W., Wang, Z., Ruhl, E. & Brutschy, B. (1987). *J. Chem. Phys.* **86**, 2525–2259.
Kato, M., Morishita, Y., Koike, F., Fritzsche, S., Yamaoka, H., Tamenori, Y., Okada, K., Matsudo, T., Gejo, T., Suzuke, I. H. & Saito, N. (2006). *J. Phys. B*, **39**, 2059–2069.
Maeda, K., Ueda, K. & Ito, K. (1993). *J. Phys. B*, **26**, 1541–1555.
Miescher, E., Lee, Y. T. & Gürtler, P. (1978). *J. Chem. Phys.* **68**, 2753–2756.
Ng, C. Y. (2000). *Int. J. Mass Spectrom.* **200**, 357–386.
Ono, Y., Linn, S. H., Prest, H. F., Ng, C. Y. & Miescher, E. (1980). *J. Chem. Phys.* **73**, 4855–4861.
Qi, F., Yang, X., Yang, S. H., Liu, F. Y., Sheng, L. S., Gao, H., Zhang, Y. W. & Yu, S. Q. (1997). *J. Chem. Phys.* **106**, 9474–9482.
Sairanen, O. P., Kivimaki, A., Nommiste, E., Aksela, H. & Aksela, S. (1996). *Phys. Rev. A*, **54**, 2834–2839.
Schmoranzer, H., Lauuer, S., Liebel, H., Ehresmann, A., Demekhin, P. V., Lagutin, B. M., Petrov, I. D. & Sukhorukov, V. L. (2001). *J. Electron. Spectrosc. Relat. Phenom.* **114–116**, 135–140.
Schulz, K., Domke, M., Puttner, R., Gutiérrez, A. & Kaindl, G. (1996). *Phys. Rev. A*, **54**, 3095–3112.
Shaw, D. A., Holland, D. M. P., MacDonald, M. A., Hayes, M. A., Shpinkova, L. G., Rennie, E. E., Johnson, C. A. F., Parker, J. E. & von Niessen, W. (1998). *Chem. Phys.* **230**, 97–116.
Tseng, P. C., Lin, H. J., Chung, S. C. Chen, C. I., Lin, H. F., Dann, T. E., Song, Y. F., Hsieh, T. F., Tsang, K. L. & Chang, C. N. (1995). *Rev. Sci. Instrum.* **66**, 1658–1660.
Zhang, Y. W., Sheng, L. S., Gao, H. & Zhang, G. B. (2003). *Nucl. Tech.* **26**, 489–493.